Model Predictive Control of Robot Flexible Joint Motor Based on Lyapunov Prediction Model

Zebin Yang, Tianyang Shen, Xiaodong Sun, *Senior Member, IEEE*, Hao Xu, and Wei Pan

***Abstract*—To address the parameter sensitivity issue of flexible joint permanent magnet synchronous motors (FJ-PMSMs) when employing a candidate voltage vector strategy, an adaptive method based on the Lyapunov function predictive model is proposed. By using the finite control set model predictive control (FCS-MPC) approach, the continuous input control law is transformed into relevant constraints of the FCS-MPC optimization problem. Specific equations are constructed through online adaptive laws to ensure system robustness, thereby tracking performance and minimizing current ripple. The effectiveness of the strategy is verified by experiments, the proposed strategy is compared with conventional MPC control methods. It effectively resolved the parameter uncertainties and load disturbance issues of the FJ-PMSM, showing superior current quality over traditional methods.**

***Index Terms*—Candidate voltage vectors, finite control set model predictive control (FCS-MPC), flexible joint permanent magnet synchronous motors (FJ-PMSMs), flexible joint permanent magnet synchronous motor, robustness.**

I. Introduction

IN MOTION control systems such as industrial robots and aerospace structural drives, lightweight, and high self-weight structural materials are commonly used to reduce their own weight. These structures undergo changes during motion, causing corresponding stresses, and exhibiting typical flexible load characteristics. Modeling and robust control of articulated robots are essential in response to this situation [1]. More and more robots are equipped with flexible joints, enabling them to maneuver and operate flexibly in complex environments, while reducing the risk of collisions and damage to the robot and its surrounding environment.

Compared with rigid joints, flexible joints are better at adapting to irregular shapes and surfaces, thereby enhancing the adaptability and safety of robots in human-computer interaction.

Generally speaking, a flexible joint permanent magnet synchronous motor (FJ-PMSM) consists of a drive motor, a flexible reduction device, and a connecting rod at the load end.

Received 10 October 2024; revised 5 February 2025; accepted 28 March 2025. Date of publication 1 April 2025; date of current version 26 May 2025. This work was supported by the Key Research and Development Program of Jiangsu Province under Grant BE2023052. Recommended for publication by Associate Editor A. Yazdani. *(Corresponding author: Xiaodong Sun.)*

Zebin Yang, Tianyang Shen, Hao Xu, and Wei Pan are with the School of Electrical and Information Engineering, Jiangsu University, Zhenjiang 212013, China (e-mail: zbyang@ujs.edu.cn; 2222307120@stmail.ujs.edu.cn; 2212307024@stmail.ujs.edu.cn; 1000002634@ujs.edu.cn).

Xiaodong Sun is with the Automotive Engineering Research Institute, Jiangsu University, Zhenjiang 212013, China (e-mail: xdsun@ujs.edu.cn).

Color versions of one or more figures in this article are available at https://doi.org/10.1109/TPEL.2025.3556654.

Digital Object Identifier 10.1109/TPEL.2025.3556654

Compared with asynchronous motors, the efficiency and power factor of permanent magnet synchronous motors are greatly improved because no reactive excitation current is required [2], [3]. Compared with ordinary synchronous motors, the rotor winding excitation device is replaced by permanent magnets, which simplifies the motor structure and improves efficiency. At present, researchers worldwide generally use excellent control methods such as vector control [4], [5], direct torque control [6], [7], and model predictive control [8], [9], [10] to carry out high-precision, high-dynamic performance, and wide-range speed regulation or positioning control of permanent magnet synchronous motors. However, in this context, the control design of the voltage source inverter-fed PMSM driver is still a very challenging task, and the nonlinear term coupling in the model [11], the discrete nature of the VSI [12], and the uncertainty of the motor parameters [13], [14], [15], [16] bring great difficulties to achieve the goal of high control performance.

In contemporary research, analogous to controlling FJ-PMSM, the techniques for controlling the speed of VSI-fed PMSM drivers can primarily be classified into two categories: 1) continuous input and 2) discrete input methodologies [17], [18]. The former, often referred to as the indirect method, achieves speed regulation through modulating the pulsewidth modulation (PWM) switching frequency [19]. This foundational principle has paved the way for several sophisticated nonlinear control strategies, including fuzzy logic control (FLC) [20], neural network control (NNC), sliding mode control (SMC) [21], [22], adaptive control [23], [24], and nonlinear optimal control [25], [26].

Among the various methods mentioned above, each possesses its own advantages and disadvantages. FLC demonstrates a commendable ability to adapt to uncertainties and complexities, offering satisfactory control performance for motor systems that are difficult to model or exhibit significant parameter variations. Due to its nonlinear nature, FLC exhibits strong robustness against changes in system parameters and external disturbances. However, it falls short in terms of computational complexity, introducing additional computational overhead in real-time control systems, which significantly increases computation time. NNC has shown extraordinary capability in adapting to the nonlinear, time-varying characteristics and uncertainties within motor drive systems. Although, it can withstand the effects of parameter changes, noise, and external disturbances to some extent, it is somewhat less effective compared to other methods. Moreover, NNC requires substantial computational resources, necessitating high-performance hardware to meet real-time

requirements. While SMC provides robustness for bounded parameters, it still faces challenges in addressing chattering issues. Adaptive control methods offer stability assurance laws without considering unknown parameters. Adaptive laws can be flexibly applied to PID gains, compensation terms, or selected parameters of the model. Despite the flexibility in adaptive control design, many current literatures inadequately address critical issues such as optimality constraints, adjustment of adaptive gains, and related parameters [27], [28], [29], [30].

To enhance robustness and stability while avoiding excessive computational complexity, an adaptive method based on the Lyapunov function predictive model is proposed. By establishing a continuous control law approach, the robustness of the continuous control law is embedded within the discrete control law as an additional constraint. Online adaptive laws ensure robustness by employing online identification algorithms to estimate motor parameters, which are then utilized in the design of the control strategy. This approach is grounded in a specific form of error feedback mechanism, whereby parameters are adjusted in real-time based on the error, effectively mitigating the impact of parameter variations. Stability is achieved through the implementation of feedback control laws. To date, this process not only guarantees system stability and robustness but also satisfies the flexibility required by model predictive control [31], [32] for various metrics. Regarding reference voltage vectors, numerous schemes have been proposed by scholars both domestically and internationally [33], [34], [35], [36], such as synthesizing reference vectors from two or three basic voltage vectors (considering zero vectors), adjusting the duty cycle to synthesize optimal voltage vectors, or employing the principle of deadbeat control to synthesize optimal voltage vectors [37], [38], [39], [40]. In brief, the approach of selecting reference voltage vectors aims to apply the ideal voltage to the stator windings of the motor to generate the desired flux and torque. Given that this method inherently involves significant computational requirements, choosing an appropriate synthesis method and the number of vectors becomes particularly critical. This issue is effectively addressed in this article. This article adopts an improved technique based on discrete space vector modulation (DSVM), which synthesizes virtual voltage vectors within a single sampling period to improve motor drive performance. Although the increase in voltage vectors can lead to greater complexity in enumerating computation tables and switching tables, the improved control strategy using DSVM technology can reduce torque ripple and computational load [41], [42]. In this strategy, three feasible voltage vectors adjacent to the optimal voltage vector are selected as candidate voltage vectors according to the cost function [43], [44], [45]. The positioning of the optimal voltage vector is calculated to lower computational costs.

In the control system of FJ-PMSM, it is common to equip the motor with a reducer. When operating under load for extended periods, the motor temperature tends to be high, leading to more pronounced parameter variations. Additionally, the high precision requirements of robotic arms necessitate stringent demands on the torque ripple of FJ-PMSM. The robustness and minimal torque ripple offered by the proposed approach adequately meet the requirements of the control system, enabling FJ-PMSM to exhibit superior control performance during practical operations. This contributes significantly to the advancement of system control for FJ-PMSM. The strong robustness ensures reliable operation despite parameter changes due to temperature fluctuations, while the reduced torque ripple supports the high-precision positioning required in robotic applications. Therefore, the implementation of this method enhances the overall performance and reliability of FJ-PMSM systems, fostering further developments in their control methodologies.

II. Mathematical Model of FJ-PMSM

The three-phase FJ-PMSM mathematical model is established in the synchronous rotating coordinate system (d-q). The voltage equation of stator winding is

$$\begin{cases} u_d = Ri_d + L\dot{i}_d - \omega L i_q \\ u_q = Ri_q + L\dot{i}_q + \omega L i_d + \omega\psi_m \end{cases} \tag{1}$$

where u, I, and L represent voltage, current, and inductance, respectively. The subscripts d and q represent the components in the d-q coordinate system. R, ψ_m, and ω represent stator resistance, electrical angular velocity, and flux linkage, respectively.

The electromagnetic torque equation of FJ-PMSM can be expressed as

$$T = \frac{3}{2} p i_q \psi_m \tag{2}$$

where p is the number of pole pairs of the motor.

In addition, the mechanical motion equation of the motor is

$$T - T_L = \frac{J}{P}\dot{\omega} + B\omega. \tag{3}$$

This section derives a dynamic model with uncertain parameters for an SPMSM drive.

The dynamic model of the SPMSM in the synchronously rotating $d-q$ reference frame is presented as follows:

$$\begin{cases} \dot{i}_d = -a_1 i_d + a_2 u_d + \omega i_q - d_d \\ \dot{i}_q = -a_1 i_q + a_2 u_q - \omega i_d - a_3\omega - d_q \\ \dot{\omega} = a_4 i_q - a_5\omega - a_6 T_L \end{cases} \tag{4}$$

where $a_1 = \frac{R}{L}, a_2 = \frac{1}{L}, a_3 = \frac{\psi_m}{L}, a_4 = \frac{3p^2\psi_m}{2J}, a_5 = \frac{B}{J}, a_6 = \frac{p}{J}$, J is the moment of inertia, B is the viscous friction coefficient, In the dynamic model (4), d_d, d_q, and d_ω represent slowly changing disturbances, and T_L represents the load torque.

In this article, the proposed method simplifies the model with only two equations to reduce the dynamic order with a new state variable z defined as

$$\begin{cases} \omega_e = \omega - \omega_d \\ z = \dot{\omega} = a_4 i_q - a_5\omega - a_6 T_L \end{cases} \tag{5}$$

where ω_e is the speed error and ω_d is the reference rotor speed. The stability target for ω_e at 0 is interpreted as the stability of z at 0. Take the derivative of (5), insert (4) into the new equation

$$\begin{cases} \dot{\omega}_e = \dot{\omega} - \dot{\omega}_d \\ \dot{z} = a_4(-a_1 i_q + a_2 V_q - \omega i_d - a_3\omega - d_q) - a_5\dot{\omega} - a_6\dot{T}_L \end{cases}. \tag{6}$$

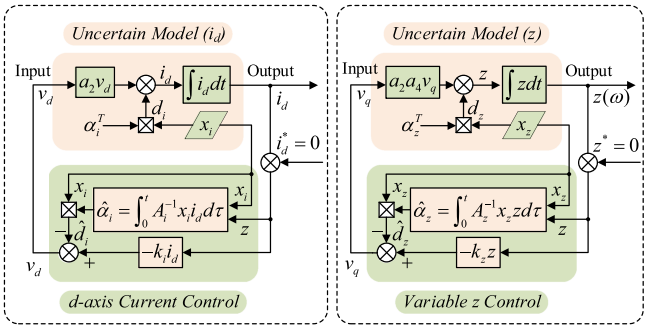

Fig. 1. Proposed method flowchart.

In the actual operating case, the speed, load torque, and *dq*-axis disturbances are slow and therefore negligible, and the assumptions are made to remove the irrelevant terms from the equation, and (6) can be reduced to

$$\begin{cases} \dot{\omega}_e = \dot{\omega} = z \\ \dot{z} = -a_5 z - a_1 a_4 i_q + a_2 a_4 V_q - a_4 \omega i_d - a_3 a_4 \omega \end{cases}. \tag{7}$$

III. Proposed Scheme

A. Uncertainty of FJ-PMSM

In this article, the second-order system that can be obtained from (4) and (7) is

$$\begin{cases} \beta = a_2 a_4 (V_q - \alpha_z^T x_z) \\ \dot{i}_d = a_2 (V_d - \alpha_i^T x_i) \end{cases} \tag{8}$$

where

$$x_z = \begin{bmatrix} i_q & \omega i_d & \omega & 1 \end{bmatrix}^T$$

$$x_i = \begin{bmatrix} i_d & \omega i_q & 1 \end{bmatrix}^T$$

α_i, α_z represent vectors of unknown parameters. The above second-order dynamic model is simplified to a first-order dynamic model, and the new dynamic model of SPMSM is

$$\dot{i}_d = a_2 (u_d - \alpha_i^T x_i), \dot{z} = a_2 a_4 (u_q - \alpha_z^T x_z). \tag{9}$$

Applying the adaptive and feedback control laws, (9) must be stable at the origin, and under normal circumstances, the controller can be designed to

$$u_d = -k_i i_d + \hat{\alpha}_i^T x_i, u_q = -k_z z + \hat{\alpha}_z^T x_z \tag{10}$$

where $k_i > 0$, $k_z > 0$ is the feedback coefficient,$\hat{\alpha}_i^T$, $\hat{\alpha}_z^T$ are, respectively, the adaptive terms of ${\alpha_i}^T$, ${\alpha_z}^T$, thus, in combination with (10), as shown in Fig. 1, the original (9) can be expressed as

$$\dot{i}_d = a_2 (-k_i i_d - \Delta\alpha_i^T x_i), \dot{z} = a_2 a_4 (-k_z z - \Delta\alpha_z^T x_z). \tag{11}$$

The control law based on the Lyapunov function can be written as

$$V(t) = \frac{i_d^2}{2} + \frac{a_2 \Delta\alpha_i^T A_i \Delta\alpha_i}{2} + \frac{z^2}{2} + \frac{a_2 a_4 \Delta\alpha_z^T A_z \Delta\alpha_z}{2} > 0 \tag{12}$$

where A_i, A_z is invertible positive definite matrix, so taking the derivative of (12) gives you the first-time derivative of CLF

$$\begin{aligned} \dot{V}(t) = & -a_2 k_i i_d^2 - a_2 a_4 k_z z^2 \\ & - a_2 (\Delta\alpha_i^T x_i i_d + \Delta\alpha_i^T A_i \dot{\hat{\alpha}}_i) \\ & - a_2 a_4 (\Delta\alpha_z^T x_z z + \Delta\alpha_z^T A_z \dot{\hat{\alpha}}_z). \end{aligned} \tag{13}$$

Set the parentheses equal to zero, then

$$\begin{cases} \dot{\hat{\alpha}}_i = -A_i^{-1} x_i i_d \Leftrightarrow \hat{\alpha}_i = -\int_0^t A_i^{-1} x_i i_d d\tau + \hat{\alpha}_i(0) \\ \dot{\hat{\alpha}}_z = -A_z^{-1} x_z z \Leftrightarrow \hat{\alpha}_z = -\int_0^t A_z^{-1} x_z z d\tau + \hat{\alpha}_z(0) \end{cases} \tag{14}$$

where $\hat{\alpha}_i(0), \hat{\alpha}_z(0)$ are Initial values. The adaptive law contributes to the stability of the feedback control law by compensating for the uncertainty d_i, d_z. Then, (13) can be rewritten as

$$\dot{V}(t) = -a_2 k_i i_d^2 - a_2 a_4 k_z z^2 < 0. \tag{15}$$

where *V(t)* decreases monotonically over (0, +∞), it can be obtained by (12) that V(t) ≤ V(0) < ∞, integrate both sides of (15), it can be written as

$$\begin{aligned} a_2 k_i \int_0^\infty i_d^2 dt + a_2 a_4 k_z \int_0^\infty z^2 dt = V(0) - V(\infty) \sqrt{b^2 - 4ac} \\ < V(0) < \infty. \end{aligned} \tag{16}$$

The following equation is inferred from (16):

$$\int_0^\infty i_d^2 dt < \infty, \int_0^\infty z^2 dt < \infty. \tag{17}$$

From (17), it can be obtained by Babarlat lemma that i_d, z converges to 0, i.e., the *d*-axis current and torque converge to the reference value, and the control law can be stabilized at the origin.

B. Stability of Discrete Input Systems

The continuous control law (10) can be directly applied by the SVPWM technique, and the sector modulation principle of the reference vector $V_s = (V_q{}^*, V_d{}^*)$ is derived by combining the fundamental voltage vector ($V_s{}^r$, $V_s{}^l$, $V_s{}^0$)

$$\begin{bmatrix} V_d{}^* \\ V_q{}^* \end{bmatrix} = \alpha \begin{bmatrix} V_d^r \\ V_q^r \end{bmatrix} + \beta \begin{bmatrix} V_d^l \\ V_q^l \end{bmatrix} + (1 - \alpha - \beta) \begin{bmatrix} V_d^0 \\ V_q^0 \end{bmatrix} \tag{18}$$

where $\alpha \geq 0$, $\beta \geq 0$, $\alpha + \beta \leq 1$, In the equation, the superscript (0, *r*, *l*) represents the zero, right, and left vectors in the reference sector, respectively.

If there is a viable continuous reference vector in (10) that guarantees the stability of (9), then there is at least one elementary discrete vector in the selected sector such that (9) is also stable.

In (18), as a feasible reference vector for SVPWM, the continuous control law (10) can be changed to

$$k_i{}^* = \frac{-u_d{}^* + \hat{\alpha}_i^T x_i}{i_d}, k_z{}^* = \frac{-u_q{}^* + \hat{\alpha}_z^T x_z}{z}. \tag{19}$$

Bringing (18) into (19) and (15), the first derivative of the continuous reference vector can be expressed as

$$\begin{aligned}\dot{V}\left(t,V_s^*\right) =& -a_2k_i{}^*i_d^2-a_0a_2k_z{}^*z^2\\ =&\alpha\dot{V}\left(t,V_s^r\right)+\beta\dot{V}\left(t,V_s^l\right)+\left(1-\alpha-\beta\right)\dot{V}\left(t,V_s^0\right)\end{aligned} \tag{20}$$

where $\dot{V}(t,V_s^r)$, $\dot{V}(t,V_s^l)$, and $\dot{V}(t,V_s^0)$ are the first derivatives for the right, left, and zero vectors, respectively.

According to (19), the stability condition of the reference vectors $\dot{V}(t,V_s{}^*)<0$ and $\alpha\geq 0$, $\beta\geq 0$, $\alpha+\beta\leq 1$ is true, so there must be a negative term in$\dot{V}(t,V_s^r)$, $\dot{V}(t,V_s^l)$, and $\dot{V}(t,V_s^0)$, i.e., at least one fundamental vector in $\dot{V}(t,V_s^r)$, $\dot{V}(t,V_s^l)$, and $\dot{V}(t,V_s^0)$satisfies the stability condition of the continuous reference vector $V_s{}^*$.

C. Virtual Voltage Vectors Syntheses

According to the DSVM principle, a virtual voltage vector is synthesized by applying multiple voltage vectors at predetermined time intervals during each sampling cycle. A sampling period is divided into N parts on average, and the expression of the virtual voltage vector is

$$u^{vir}=\sum_{j=1,2,\ldots,N}t_jV_j^{\text{real}} \tag{21}$$

where

$$\begin{aligned}&V_j^{\text{real}}\in\{V_1,V_2,\ldots,V_7\}\\ &t_j=\frac{T_s}{N}\\ &n_{\text{total}}=3N^2+3N+2.\end{aligned} \tag{22}$$

For example, "*66Z*" refers to the fundamental voltage vectors U_6 and U_0 with 2/3 and 1/3 sampling periods applied respectively, and "*46Z*" refers to the fundamental voltage vectors U_4, U_6, and U_0 with 1/3 of the sampling period applied, respectively.

The required virtual voltage vector can be calculated in reverse from the reference torque and flux, and the virtual voltage vector can be solved as follows: the difference between the torque at *k + 1* and *k + 2* can be expressed as

$$\Delta T\left(k+1\right)=T\left(k+2\right)-T\left(k+1\right). \tag{23}$$

Therefore, the expression for the change of the virtual vector and the torque is (24), where a and b are the components of the virtual voltage vector in the *d*-axis and *q*-axis

$$V_q\left(k+1\right)T_s=MV_d\left(k+1\right)T_s+B \tag{24}$$

where

$$M=\frac{\left(L_d-L_q\right)\psi_q\left(k+1\right)}{\left(L_d-L_q\right)\psi_d\left(k+1\right)+L_d\psi_m}$$

$$\begin{aligned}B=&\frac{L_dL_q}{\left(L_d-L_q\right)\psi_d\left(k+1\right)+L_q\psi_m}\left[\frac{4\Delta T\left(k+1\right)}{3p}\right.\\ &-\frac{\omega T_s}{L_dL_q}\left(\left(L_q-L_d\right)\left(\psi_d^2\left(k+1\right)-\psi_q^2\left(k+1\right)\right)\right.\\ &\left.\left.-L_d\psi_d\left(k+1\right)\psi_m\right)-\frac{RT_s\psi_q\left(k+1\right)}{L_d^2L_q^2}\right.\\ &\left.\left(\left(L_q^2-L_d^2\right)\psi_d\left(k+1\right)-L_q^2\psi_m\right)\right]\\ =&\frac{L}{\psi_m}\left[\frac{4\Delta T\left(k+1\right)}{3p}+\frac{\omega T_s}{L}\psi_d\left(k+1\right)\psi_m\right.\\ &\left.+\frac{\mathrm{RT_s}}{\mathrm{L}^2}\psi_{\mathrm{q}}\left(\mathrm{k}+1\right)\psi_{\mathrm{m}}\right].\end{aligned}$$

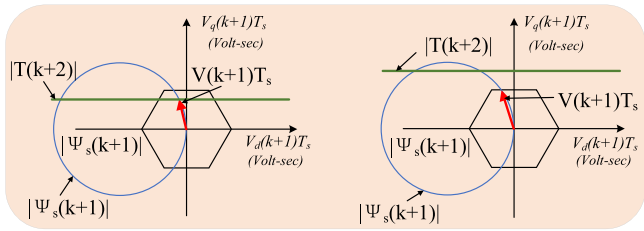

Fig. 2. Geometric solution of virtual vectors.

According to (26), Fig. 2. can be made on a plane, the torque equation is represented by a straight line. All voltage vectors in a straight line produce a corresponding torque change. Ignoring the stator resistance term, the flux equation can be approximated as

$$\psi_s\left(k+1\right)=\psi_s\left(k\right)+u_s\left(k\right)T_s. \tag{25}$$

From this, it can be deduced that the expression of the stator flux is

$$\begin{aligned}\psi_s^2\left(k+2\right)=&\psi_d^2\left(k+2\right)+\psi_q^2\left(k+2\right)\\ =&\left(\psi_d\left(k+1\right)+V_d\left(k+1\right)T_s\right)^2\\ &+\left(\psi_q\left(k+1\right)+V_q\left(k+1\right)T_s\right)^2.\end{aligned} \tag{26}$$

Equation (26) is the expression of a circle, the center of the circle is $[-\psi_d(k+1), -\psi_q(k+1)]$, the radius is $|\psi_s(k+2)|$, and it can be seen in the figure that the voltage vector represented at the intersection of the circle and the line satisfies the requirements of both torque and flux. In addition, the hexagon in the diagram represents the voltage limit of the inverter, as shown in Fig. 2, the intersection falls inside the hexagon, indicating that the inverter can output a voltage vector that satisfies both torque and flux at the same time. If the intersection falls outside the hexagon, the required voltage vector is beyond the limit that the inverter can provide, so only the intersection point and the origin can be connected, and the intersection point with the hexagon is the alternative voltage vector.

D. Improved Discrete Space-Vector Modulation Technique

According to the method of synthesizing virtual vectors from three vectors, the space of the fundamental voltage vector is divided into the region, as shown in the Fig. 3, and the three numbers on the three vertices of each triangle represent the three vectors synthesized by the vector, where *Z* represents the zero vector. After synthesizing the virtual vectors, according to the different triangles where the vertices of the virtual vectors are

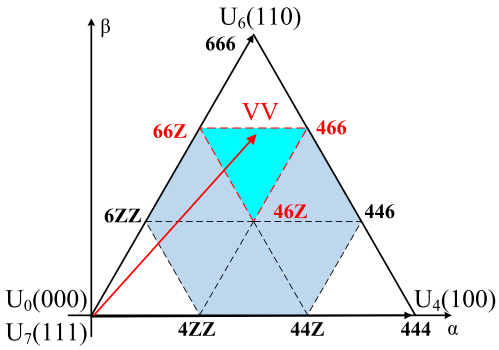

Fig. 3. Local virtual vector representation.

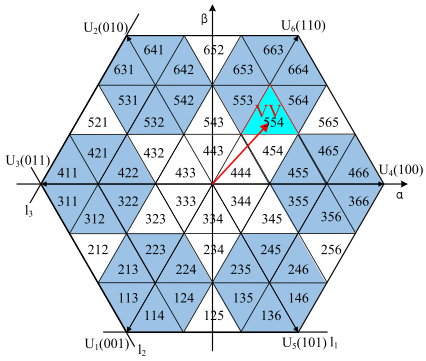

Fig. 4. Determination of the position of virtual vectors.

located, the candidate voltage vectors are increased from 6 to 38, which greatly optimizes the selection of the voltage vectors and makes the control performance of the motor better.

For the virtual vectors that need to be synthesized, an algebraic method for calculating candidate voltage vectors can be used to reduce the scope of cost function enumeration and reduce the computational burden of the system.

Assuming that l_1, l_2, and l_3 are the three boundaries of the voltage limit, as shown in the Fig. 4, the end coordinates of the virtual voltage vector can be written as (u_α, u_β), and for boundary l_1, the distance l_1 from the vertex to the boundary d_1 is

$$d_1 = \frac{u_\beta + 3u_l}{u_l} = \frac{3\left(\sqrt{3}u_\beta + u_{\mathrm{dc}}\right)}{u_{\mathrm{dc}}}. \tag{27}$$

For boundary l_2, a new coordinate system α'– β' can be constructed, where

$$u_{\beta'} = \frac{\sqrt{3}}{2}\alpha + \frac{1}{2}\beta. \tag{28}$$

According to (28), it can be inferred that the distance d_2 from the vertex to the boundary l_2 is

$$d_2 = \frac{3\left(\sqrt{3}u_{\beta'} + u_{\mathrm{dc}}\right)}{u_{\mathrm{dc}}} = \frac{3\left(\frac{3}{2}u_\alpha + \frac{\sqrt{3}}{2}u_\beta + u_{\mathrm{dc}}\right)}{u_{\mathrm{dc}}}. \tag{29}$$

In the same way, it can be inferred that the distance d_3 from the vertex to the boundary l_3 is

$$d_3 = \frac{3\left(\frac{3}{2}u_\alpha - \frac{\sqrt{3}}{2}u_\beta + u_{\mathrm{dc}}\right)}{u_{\mathrm{dc}}}. \tag{30}$$

The results of (28), (29), and (30) are rounded up to give D_1, D_2, and D_3, so the triangle containing the vertices of the virtual voltage vector can be represented as

$$D = 100D_1 + 10D_2 + D_3. \tag{31}$$

Because there is a fixed correspondence between the triangle number shown in Fig. 4 and the candidate vector synthesized with the fundamental voltage vector, i.e., the three vertices of each triangle, the corresponding table can be entered, so that according to the number of the triangle where the virtual vector is located, the corresponding candidate vector is directly brought into the cost function, and the candidate vector with the youngest value function is taken as the optimal voltage vector output.

E. MPC With Stability–Robustness Constraints

In order to achieve the above control objectives, the set cost function can be written as

$$g = A{i_d}^{*2} + Bz^{*2} \tag{32}$$

where A and B are positive weight factors according to different performance requirements. The items with superscripts $(*)$ represent the value of one-step prediction $(k+1)$, while the items without superscripts $(*)$ represent the current value of (k). In order to achieve the minimum value of the above cost function while satisfying the stability robustness constraint, (32) must satisfy the following conditions:

$$\begin{cases} k_i = \frac{-u_d + \hat{\alpha}_i^T x_i}{i_d} > 0 \\ k_z = \frac{-u_q + \hat{\alpha}_z^T x_z}{z} > 0. \end{cases} \tag{33}$$

Depending on the predicted value, ${i_d}^*$ and z^* in (32) can be written as

$$\begin{cases} {i_d}^* = i_d(k) + T_s a_2(u_d + \hat{d}_i) \\ z^* = z\,(k) + T_s a_2 a_4\left(u_q + \hat{d}_z\right) \end{cases} \tag{34}$$

where T_s is the sampling period.

In the abovementioned formula, $i_d(k)$ represents the current at the sampling time, and ${i_d}^*$ represents the predicted value after one step of prediction, which is also applicable to z.

The FCS-MPC optimization problem according to (14), (32), and (33) has certain advantages, first, the robustness of the control is guaranteed by (14), the stability is guaranteed by the symbol of two feedback gains, and by setting the appropriate optimal criterion, a number of important parameters (such as motor torque ripple, switching frequency, power loss, and maximum output current) are flexibly controlled to achieve multiobjective optimal control.

In summary, Fig. 5 shows the overall experimental flowchart of FCS-MPC. As shown in the figure, the proposed optimization scheme is derived from the basic d-q model, which transforms

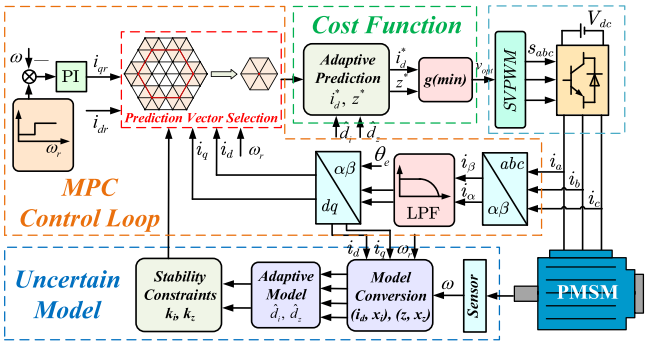

Fig. 5. FCS-MPC overall control block diagram.

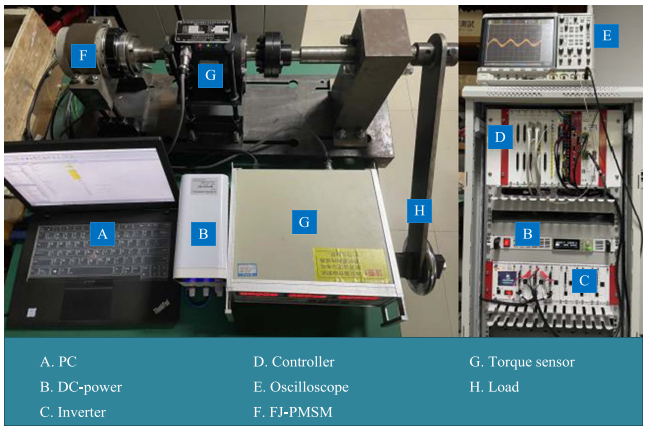

Fig. 6. Experimental setup.

the model by using new state variables, and finally simplifies according to relevant constraints. The adaptive law with a lumped adaptive quantity ensures the robustness of the model. Through this adaptive term, the stability robustness constraints (k_i, k_z) and predicted state variables ($i_d{}^*$, z^*) of the switching states in a finite set are calculated online using (33) and (34). Finally, based on the selection of the optimal voltage vector, the FCS-MPC obtains the optimal switching state S_{abc}, which is then handed over to the PWM module to control the on/off of the IGBT.

IV. Simulation and Experiment Verification

A. Experimental Setup

To verify the feasibility of the proposed method in practical applications, we constructed a flexible joint experimental platform, as shown in Fig. 6, for validation. The platform includes a cascaded arrangement of FJ-PMSM, torque sensors, and drive chains. At the output end, the connecting rod connected by flanges allows for load exchange, allowing the load on the flexible joint to be changed according to experimental conditions. This facilitates the verification of the tracking performance of the system under different loads.

The control system of the experimental platform consists of a real-time controller RTU-BOX, a power converter, and a power module. The control platform supports real-time operating systems, ensuring high-precision time management during the control process and meeting the requirements of time sensitive control tasks. And the platform has built-in data collection and monitoring functions, which can monitor and analyze the system's operating status in real time. Users can monitor various parameters of the system through a graphical interface. The measurement value of the torque sensor is only for reference purposes and is not fed back to the controller. The position signals from the motor side and the chain side are fed back to the controller through position sensors. The controller calculates the motor drive signal based on the designed model and outputs it to the power converter to drive the combined motor. Table I lists the physical parameters of FJ-PMSM.

TABLE I
PMSM System Parameters

Parameter	Sy mbol	Value
Number of pole pairs	n_p	10
d-axis inductance	L_d	0.18 mH
q-axis inductance	L_q	0.18 mH
Stator resistance	Rs	0.19 Ω
Permanent-magnet flux linkage	ψ_f	0.0053819Wb
Dc-link voltage	U_{dc}	48 V
Rated speed	N	3500 r/min
Rated power	P_N	400 W
Inertia	J	0.0000376 kgm2
Reduction ratio	R_r	100:1

B. Impact of Stability-Robustness Constraints on Performance

During this process, the sampling frequency of all control experiments was controlled at 10 kHz. The parameter design of the speed controller is set to Kp = 0.31 and Ki = 20.

First, some statements need to be made here. Due to the built-in reduction ratio Rr of 100:1 in the FJ-PMSM, we cannot fully simulate the no-load operation of the motor in subsequent experiments. We can only simulate the situation of variable load by increasing the load on the connecting shaft. Therefore, in subsequent experiments, the no-load mentioned by us refers to the situation where the FJ-PMSM is equipped with a reduction ratio Rr without additional load.

This article first studies the performance of the motor under sudden rated load at a rated speed of 3500 r/min and no parameter mismatch under no-load conditions. As shown in Fig. 7, the motor first runs at 3500 r/min without load. From Fig. 7, it can be seen that compared with the proposed control method, the traditional MPC control method obtains slightly poorer current quality. Due to the traditional control method of MPC using 7 basic voltage vector selections, while the method proposed in this article uses 38 candidate voltage vector selections.

In subsequent experiments, this article studied the current performance of these two different control methods under system parameter mismatch conditions. In the first set of experiments, the control condition was L′ = 2L. It can be clearly seen from Fig. 8 that the traditional MPC control method has a larger current ripple in the case of inductor configuration, while the current ripple is relatively smaller after using the control method proposed in this article. As is well known, in traditional MPC control methods, the accuracy of system parameters is highly

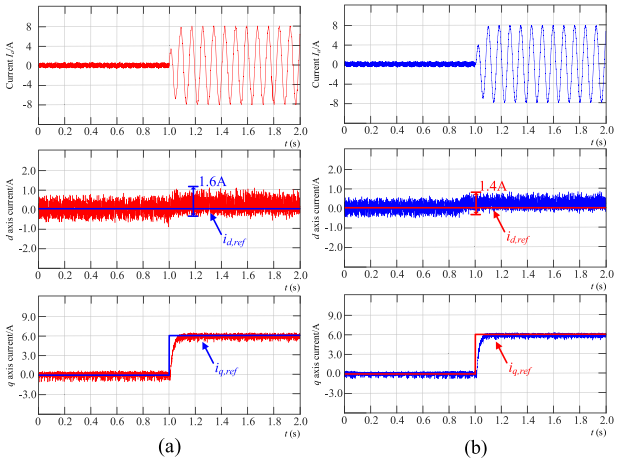

Fig. 7. Experimental performance without system parameter mismatch. (a) Traditional MPC method. (b) Proposed method.

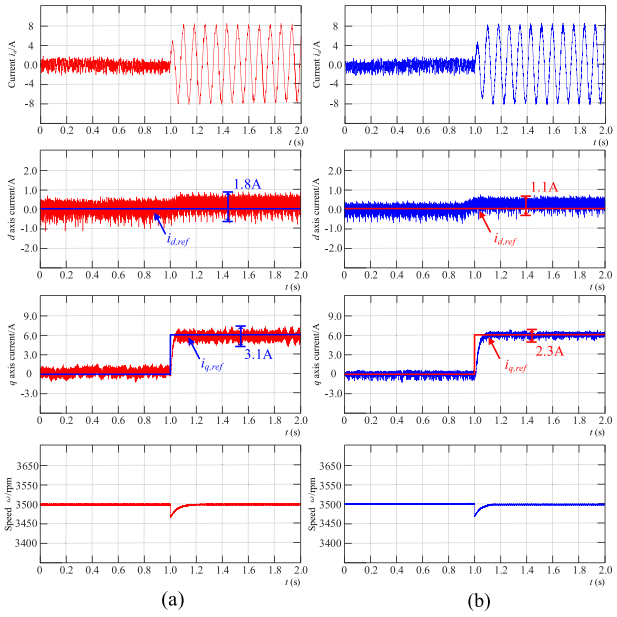

Fig. 8. Experimental performance of three methods when inductance parameter mismatch $L' = 2L$. (a) Traditional MPC method. (b) Proposed method.

required for the predicted values. The mismatch of inductance parameters may result in the selected voltage vector not being the optimal voltage vector, leading to a significant decrease in the control performance of the motor. In this article, stability assurance constraints are used to reduce the sensitivity of measurement parameters. When the system suddenly increases the load, although the motor speed slightly decreases, it can quickly follow the reference value and return to normal in a short time, and the torque ripple amplitude is also smaller than traditional MPC control methods. Although the method proposed in this article has the above advantages, traditional MPC control methods have advantages in the time required for q-axis current and motor speed to reach steady state.

The second set of experiments will change the controlled conditions to $\psi' = 2\psi$. From Fig. 9, it can be seen that the traditional MPC control method has some burrs at the peak of

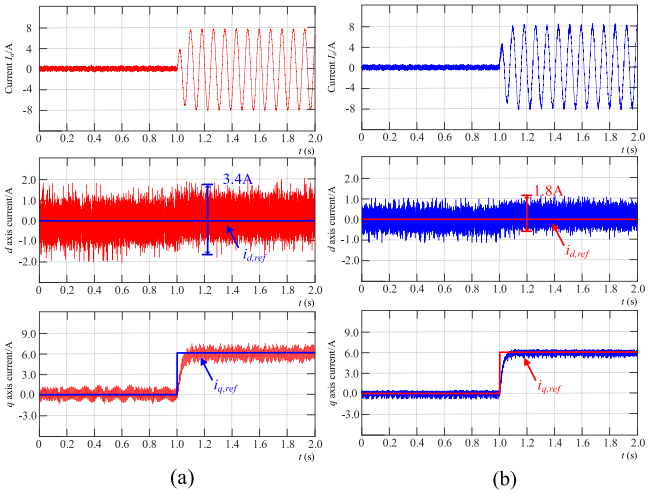

Fig. 9. Magnetic flux parameter mismatch $\psi' = 2\psi$ experimental performance of three methods. (a) Traditional MPC method. (b) Proposed method.

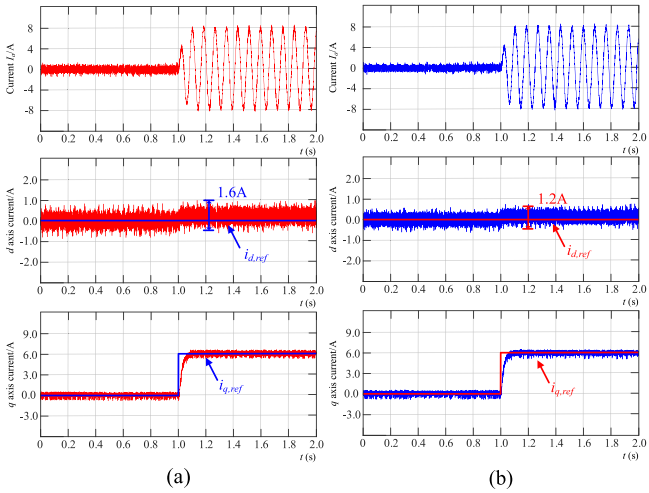

Fig. 10. Experimental performance of three methods when resistance parameter mismatch $R' = 2R$. (a) Traditional MPC method. (b) Proposed method.

the a-axis current, and the d-axis current performance deteriorates. However, proposed method in this article, due to the use of stability guaranteed constraints to reduce the sensitivity of magnetic flux parameters, the current performance is better than that of the traditional MPC control method.

The third group of experiments changed the control condition to $R' = 2R$. From Fig. 10, it can be seen that the difference between the two control methods is not significant, because the resistance parameters cannot cause a significant decrease in control performance when the system parameters are adapted. Usually, when high accuracy is required, scholars usually ignore it to simplify the model.

C. Comparison of Calculation Time Between the Proposed Method and Other Methods

To evaluate the feasibility of the real-time constraints of the proposed method, its computational demand was compared with that of existing methods. Table II provides a comparison of

TABLE II
IMPLEMENTATION COMPLEXITY OF FOUR METHODS

	FCS-MPC	DTC	MFPC	Proposed method
Required motor parameters	R_s, L_d, L_q, Ψ_f, ect	R_s, L_d, L_q, Ψ_f	None	R_s, L_d, L_q, Ψ_f, ect
Parameters to be designed	K_p, K_i	None	α, ω_0	A, B
Computing time	32.7 μs	38.5 μs	34.2 μs	34.4 μs

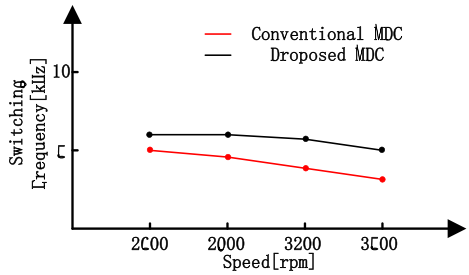

Fig. 11. Comparison between the proposed method and traditional MPC method in terms of switching frequency.

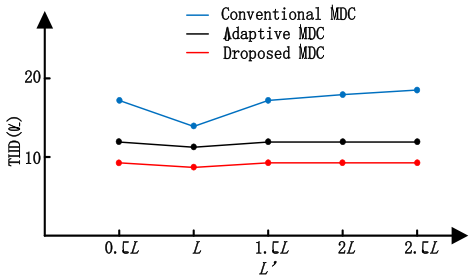

Fig. 12. Comparison of current THD measured by three different methods.

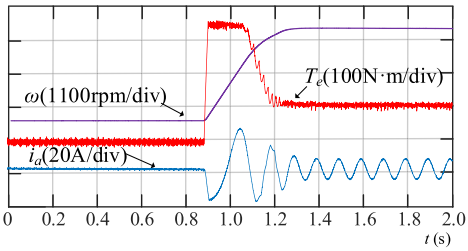

Fig. 13. Acceleration test from stationary to 3500 r/min.

implementation complexity against three alternative approaches. It is evident that, in terms of computational time, the proposed method exhibits a slight increase compared to conventional FCS-MPC, DTC, and MFPC, primarily due to the additional time required for screening candidate voltage vectors as opposed to merely enumerating basic voltage vectors. For MFPC, the proposed method requires fewer control parameters, significantly reducing the computational burden. Considering the enhanced robustness to parameter variations and the reduced torque ripple offered by the proposed method, it can be concluded that, overall, the proposed method outperforms the other three methods in comprehensive performance metrics. The increased computational time is justified by the improved system robustness and control quality, indicating that the proposed method strikes a favorable balance between computational efficiency and control effectiveness.

D. Comparative Performance Investigation

In the following control experiments, this article measured the switching frequency of these two control methods at rated load and different speeds. The conclusion drawn from Fig. 11 is that the switching frequency of the proposed control method is slightly higher than that of the traditional MPC control method.

The reason for this deviation is simple. In the process of selecting candidate voltage vectors, the control cycle is artificially divided into three equal parts, which inevitably leads to an increase in the number of switch states. It is encouraging that in subsequent control experiments, the sampling frequency was reduced to the level of traditional MPC control methods, and the control method proposed in this article has smaller current ripple compared to the former. The experimental results obtained are shown in Fig. 12, which includes an additional set of experiments on control methods based on parameter adaptive laws. The control method based on parameter adaptation and the proposed method have higher accuracy in predicting inductance parameters, therefore both have better power quality. It is evident that traditional MPC control methods are more sensitive to parameter mismatches.

From the acceleration experiment graph in Fig. 13, it can be seen that the motor accelerates from static to 3500 r/min without parameter mismatch. The waveforms of its speed, torque, and three-phase current are shown in the figure. The torque shown in Fig. 13 is obtained from the external according to the torque sensor. Due to the 100:1 speed ratio of FJ-PMSM, the externally measured torque is 100 N·m, and the internal motor body has a rated torque of 1 N·m. The speed curve is directly obtained through RTU-BOX internal monitoring, and observed from the outside, with a speed of 35 r/min. It is encouraging that the waveform of the transient speed of the motor is very smooth, and the control method proposed in this article also has smaller torque fluctuations and better current quality. In the practical application scenario of FJ-PMSM, the transient velocity waveform of the rotational speed is smooth, representing the stability of the robot arm under working conditions, and its vibration is small. Therefore, it is very meaningful for the development of subsequent research.

V. CONCLUSION

This article proposes a new method for optimizing the robustness of model predictive control based on the Lyapunov function as a cost function for stability. This method constructs a novel cost function to enhance the tracking and robustness of the control system. Has shown strong anti-interference ability in experiments. In addition, the addition of reference voltage vectors enables the model to have better trajectory tracking ability and lower switching frequency, proving its effectiveness. The experimental results show that this method has good control

stability. Future research will expand to improve the disturbance rejection capability and dynamic parameter identification of multidegree of freedom flexible joint robotic arms.

REFERENCES

[1] H. Qiu, C. Yuan, W. Chen, X. Ma, and B. Xiong, "Combined regulation performance research of the novel flux-torque regulation hybrid excitation machine with axial-radial magnetic circuit," *IEEE Trans. Transp. Electrific.*, vol. 10, no. 4, pp. 10420–10427, Dec. 2024.

[2] Z. Su, X. Sun, G. Lei, and M. Yao, "Improved model-free predictive current control for SPMSM drives with adaptive prediction horizon strategy," *IEEE Trans. Ind. Electron.*, to be published, doi: 10.1109/TIE.2024.3503594.

[3] A. Mora, Á. Orellana, J. Juliet, and R. Cárdenas, "Model predictive torque control for torque ripple compensation in variable-speed PMSMs," *IEEE Trans. Ind. Electron.*, vol. 63, no. 7, pp. 4584–4592, Jul. 2016.

[4] Z. Dong, Z. Song, W. Wang, and C. Liu, "Improved zero-sequence current hysteresis control-based space vector modulation for open-end winding PMSM drives with common DC bus," *IEEE Trans. Ind. Electron.*, vol. 70, no. 10, pp. 10755–10760, Oct. 2023.

[5] J. G. Roos and J. H. R. Enslin, "Analysis, simulation and practical evaluation of torque vector control strategies for medium power highly responsive PMSM drives," *Trans. South Afr. Inst. Elect. Engineers*, vol. 82, no. 2, pp. 135–142, Jun. 1991.

[6] M. Wang, D. Sun, W. Ke, and H. Nian, "A universal lookup table-based direct torque control for OW-PMSM drives," *IEEE Trans. Power Electron.*, vol. 36, no. 6, pp. 6188–6191, Jun. 2021.

[7] W. Deng, J. Tang, and W. Cheng, "An enhanced rotating vector-based direct torque control for matrix converter-fed PMSM drives using virtual pulsating vectors," *CPSS Trans. Power Electron. Appl.*, vol. 8, no. 1, pp. 65–73, Mar. 2023.

[8] T. Jin et al., "Low complexity model predictive flux control based on discrete space vector modulation and optimal switching sequence for induction motors," *IEEE Trans. Ind. Electron.*, vol. 71, no. 1, pp. 305–315, Jan. 2024.

[9] J. Rodriguez et al., "Latest advances of model predictive control in electrical drives—Part II: Applications and benchmarking with classical control methods," *IEEE Trans. Power Electron.*, vol. 37, no. 5, pp. 5047–5061, May 2022.

[10] T. Li, X. Sun, G. Lei, Z. Yang, Y. Guo, and J. Zhu, "Finite-control-set model predictive control of permanent magnet synchronous motor drive systems - An overview," *IEEE/CAA J. Autom. Sinica*, vol. 9, no. 12, pp. 2087–2105, Dec. 2022.

[11] G. Luo, R. Zhang, Z. Chen, W. Tu, S. Zhang, and R. Kennel, "A novel nonlinear modeling method for permanent-magnet synchronous motors," *IEEE Trans. Ind. Electron.*, vol. 63, no. 10, pp. 6490–6498, Oct. 2016.

[12] S. Wang, C. Li, C. Che, and D. Xu, "Direct torque control for 2L-VSI PMSM using switching instant table," *IEEE Trans. Ind. Electron.*, vol. 65, no. 12, pp. 9410–9420, Dec. 2018.

[13] M. Tian, B. Wang, Y. Yu, Q. Dong, and D. Xu, "Robust adaptive resonant controller for PMSM speed regulation considering uncertain periodic and aperiodic disturbances," *IEEE Trans. Ind. Electron.*, vol. 70, no. 4, pp. 3362–3372, Apr. 2023.

[14] X. Sun, Z. Su, G. Lei, and M. Yao, "Robust predictive cascaded speed and current control for PMSM drives considering parameter variations," *IEEE Trans. Ind. Electron.*, vol. 71, no. 9, pp. 10235–10245, Sep. 2024.

[15] J.-W. Jung, V. Q. Leu, T. D. Do, E.-K. Kim, and H. H. Choi, "Adaptive PID speed control design for permanent magnet synchronous motor drives," *IEEE Trans. Power Electron.*, vol. 30, no. 2, pp. 900–908, Feb. 2015.

[16] H. H. Choi, N. T.-T. Vu, and J.-W. Jung, "Digital implementation of an adaptive speed regulator for a PMSM," *IEEE Trans. Power Electron.*, vol. 26, no. 1, pp. 3–8, Jan. 2011.

[17] K. S. Alam, M. P. Akter, D. Xiao, D. Zhang, and M. F. Rahman, "Asymptotically stable predictive control of grid-connected converter based on discrete space vector modulation," *IEEE Trans. Ind. Electron.*, vol. 15, no. 5, pp. 2775–2785, May 2019.

[18] Y. Wang et al., "Deadbeat model-predictive torque control with discrete space-vector modulation for PMSM drives," *IEEE Trans. Ind. Electron.*, vol. 64, no. 5, pp. 3537–3547, May 2017.

[19] S. Yang, P. Zheng, Y. Sui, C. Tong, and M. Wang, "Carrier-based PWM technique and extended state observer-based current control scheme for current-source inverter-fed five-phase PMSM drives," *IEEE Trans. Ind. Electron.*, vol. 71, no. 7, pp. 6635–6646, Jul. 2024.

[20] Y. Shen, Z. Li, X. Tian, K. Ji, and X. Yang, "Vibration suppression of the vehicle mechatronic ISD suspension using the fractional-order biquadratic electrical network," *Fractal Fractional*, vol. 9, no. 2, 2025, Art. no. 106.

[21] M. Muthusamy, J. Hendershot, and P. Pillay, "Design of a spoke type PMSM with SMC stator core for traction applications," *IEEE Trans. Ind. Appl.*, vol. 59, no. 2, pp. 1418–1436, Mar./Apr. 2023.

[22] J. Liu, H. Li, and Y. Deng, "Torque ripple minimization of PMSM based on robust ILC via adaptive sliding mode control," *IEEE Trans. Power Electron.*, vol. 33, no. 4, pp. 3655–3671, Apr. 2018.

[23] Y. Yin et al., "Disturbance and uncertainty attenuation for speed regulation of PMSM servo system using adaptive optimal control strategy," *IEEE Trans. Transp. Electrific.*, vol. 9, no. 2, pp. 3410–3420, Jun. 2023.

[24] W. Zou, T. Shi, J. Guo, and Z. Xiang, "A novel adaptive fuzzy control scheme for a class of nonlinear planar systems under state constraints," *IEEE Trans. Circuits Syst. II, Exp. Briefs*, vol. 71, no. 2, pp. 827–831, Feb. 2024.

[25] L. N. Tan and T. C. Pham, "Optimal tracking control for PMSM with partially unknown dynamics, saturation voltages, torque, and voltage disturbances," *IEEE Trans. Ind. Electron.*, vol. 69, no. 4, pp. 3481–3491, Apr. 2022.

[26] H. T. Nguyen and J.-W. Jung, "Finite control set model predictive control to guarantee stability and robustness for surface-mounted PM synchronous motors," *IEEE Trans. Ind. Electron.*, vol. 65, no. 11, pp. 8510–8519, Nov. 2018.

[27] R. P. Aguilera and D. E. Quevedo, "Predictive control of power converters: Designs with guaranteed performance," *IEEE Trans. Ind. Inform.*, vol. 11, no. 1, pp. 53–63, Feb. 2015.

[28] M. Habibullah, D. D.-C. Lu, D. Xiao, and M. F. Rahman, "A simplified finite-state predictive direct torque control for induction motor drive," *IEEE Trans. Ind. Electron.*, vol. 63, no. 6, pp. 3964–3975, Jun. 2016.

[29] S. Niu, Y. Luo, W. Fu, and X. Zhang, "Robust model predictive control for a three-phase PMSM motor with improved control precision," *IEEE Trans. Ind. Electron.*, vol. 68, no. 1, pp. 838–849, Jan. 2021.

[30] S. J. Underwood and I. Husain, "Online parameter estimation and adaptive control of permanent-magnet synchronous machines," *IEEE Trans. Ind. Electron.*, vol. 57, no. 7, pp. 2435–2443, Jul. 2010.

[31] X. Sun, X. Lin, L. Zhang, M. Yao, and Y. Cai, "An improved torque enhancement strategy for dual three-phase PMSM based on model-free predictive current control," *IEEE Trans. Transport. Electrific.*, vol. 11, no. 1, pp. 176–187, Feb. 2025, doi: 10.1109/TTE.2024.3388375.

[32] T. Li, X. Sun, M. Yao, D. Guo, and Y. Sun, "Improved finite control set model predictive current control for permanent magnet synchronous motor with sliding mode observer," *IEEE Trans. Transport. Electrific.*, vol. 10, no. 1, pp. 699–710, Mar. 2024.

[33] X. Zhang, B. Hou, and Y. Mei, "Deadbeat predictive current control of permanent-magnet synchronous motors with stator current and disturbance observer," *IEEE Trans. Power Electron.*, vol. 32, no. 5, pp. 3818–3834, May 2017.

[34] X. Zhang and B. Hou, "Double vectors model predictive torque control without weighting factor based on voltage tracking error," *IEEE Trans. Power Electron.*, vol. 33, no. 3, pp. 2368–2380, Mar. 2018.

[35] X. Sun, Z. Su, G. Lei, Y. Cai, and M. Yao, "Adaptive model-free predictive current control for SPMSM drives with optimal virtual vector modulation," *IEEE/ASME Trans. Mechatron.*, vol. 29, no. 4, pp. 2569–2578, Aug. 2024, doi: 10.1109/TMECH.2023.3332136.

[36] Z. Su, X. Sun, G. Lei, and M. Yao, "Model-free predictive current control for dual three-phase PMSM drives with an optimal modulation pattern," *IEEE Trans. Ind. Electron.*, vol. 71, no. 9, pp. 10140–10149, Sep. 2024.

[37] X. Sun, X. Lin, D. Guo, G. Lei, and M. Yao, "Improved deadbeat predictive current control with extended state observer for dual three-phase PMSMs," *IEEE Trans. Power Electron.*, vol. 39, no. 6, pp. 6769–6782, Jun. 2024.

[38] M. Zhao, Y. Cao, C. Li, Z. Wang, T. Shi, and C. Xia, "Expanded limit boundary explicit model predictive direct speed control for PMSMs," *IEEE Trans. Power Electron.*, vol. 39, no. 5, pp. 6089–6101, May 2024.

[39] F. Yang, X. Zhao, H. Jin, X. Wang, and X. Liu, "Improved deadbeat predictive current control with embedded resonant polynomial and disturbance observer for PMSM current distortion rejection," *IEEE J. Emerg. Sel. Topics Power Electron.*, vol. 12, no. 2, pp. 1934–1945, Apr. 2024.

[40] L. Tian, X. Guo, L. Liu, S. Zhu, and N. Zong, "Variable vector model predictive control for permanent magnet synchronous motors using a single DC-link current sensor," *IEEE Trans. Power Electron.*, vol. 39, no. 5, pp. 5310–5319, May 2024.

[41] P. Rajanikanth, M. L. Parvathy, and V. K. Thippiripati, "Enhanced model predictive current control-based five-phase PMSM drive," *IEEE J. Emerg. Sel. Topics Power Electron.*, vol. 12, no. 1, pp. 838–848, Feb. 2024.

[42] Z. Zhang, X. Wang, and J. Xu, "Robust amplitude control set model predictive control with low-cost error for SPMSM based on nonlinear extended state observer," *IEEE Trans. Power Electron.*, vol. 39, no. 6, pp. 7016–7028, Jun. 2024.
[43] G. Scaglione, C. Nevoloso, G. Schettino, A. O. D. Tommaso, and R. Miceli, "A novel multiobjective finite control set model predictive control for IPMSM drive fed by a five-level cascaded H-bridge inverter," *IEEE J. Emerg. Sel. Topic Power Electron.*, vol. 12, no. 2, pp. 1959–1973, Apr. 2024.
[44] Y. Wei, H. Young, D. Ke, D. Huang, F. Wang, and J. Rodríguez, "Adaptive ultralocalized time-series for improved model-free predictive current control on PMSM drives," *IEEE Trans. Power Electron.*, vol. 39, no. 5, pp. 5155–5165, May 2024.
[45] M. S. Mubarok, T.-H. Liu, S. A. Davari, and J. Rodriguez, "Constrained predictive controllers for high-performance sensorless IPMSM drive systems with full-range speed operations," *IEEE Trans. Power Electron.*, vol. 39, no. 4, pp. 4612–4623, Apr. 2024.

Zebin Yang received the B.Sc., M.Sc., and Ph.D. degrees in electrical engineering from Jiangsu University, Zhenjiang, China, in 1999, 2004, and 2013, respectively.

He is currently a Professor with Jiangsu University, Zhenjiang, China. From 2014 to 2015, he was a Visiting Scholar with the School of Electrical, Mechanical, and Mechatronic Systems, University of Technology Sydney, Sydney, Australia. His main research interests include drives and control for motors and magnetic levitation transmission technology.

Tianyang Shen was born in Nantong, China, in Nov. 1999. He received the bachelor's degree in electrical engineering and automation in 2022 from the School of Electrical Information Engineering, Jiangsu University, Zhenjiang, China, where he is currently working toward the master's degree in electrical engineering.

His current research interest includes model predictive control of permanent magnet synchronous motors.

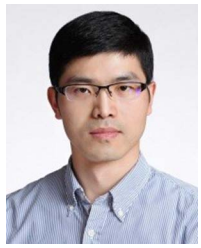

Xiaodong Sun (Senior Member, IEEE) received the B.Sc. degree in electrical engineering, and the M.Sc. and Ph.D. degrees in control engineering from Jiangsu University, Zhenjiang, China, in 2004, 2008, and 2011, respectively.

Since 2004, he has been with Jiangsu University, where he is currently a Professor in vehicle engineering with the Automotive Engineering Research Institute. From 2014 to 2015, he was a Visiting Professor with the School of Electrical, Mechanical, and Mechatronic Systems, University of Technology Sydney, Sydney, Australia. He has authored or coauthored more than 100 refereed technical papers and one book, and he is the holder of 42 patents in his areas of research interest, which include electrified vehicles, electrical machines, electrical drives, and energy management.

Dr. Sun is an Associate Editor for IEEE TRANSACTIONS ON INDUSTRIAL ELECTRONICS, Associate Editor of IEEE TRANSACTIONS ON TRANSPORTATION ELECTRIFICATION, and Editor of IEEE TRANSACTIONS ON ENERGY CONVERSION.

Hao Xu was born in Wuhai, China, in 2000. He received the B.S. degree in electrical engineering and automation from Shandong University, Jinan, China, in 2022. He is currently working toward the M.Sc. degree in electrical engineering with Jiangsu University, Zhenjiang, China.

His current research interests include algorithm control and high-efficiency operation of permanent magnet synchronous motors.

Wei Pan received B.S. and M.S. degrees in electrical engineering from China University of Mining and Technology, Xuzhou, China, in 1999, and 2002, respectively, and the Ph.D. degree in electrical engineering from Jiangsu University, Zhenjiang, China, in 2016.

She is currently an Associate Professor with Jiangsu University. Her current research interests include drives and controls for bearingless motors, and magnetic levitation transmission technology.